THETA-LIKE SPECIMEN TO DETERMINE TENSILE STRENGTH AT THE MICRO SCALE

Michael S. Gaither, Frank W. DelRio, Richard S. Gates, Edwin R. Fuller, and Robert F. Cook
National Institute of Standards and Technology, USA

ABSTRACT

Micro- and nano-electromechanical systems are typically formed via lithographic and etching processes that leave residual surface features, stresses, and chemistry that ultimately control component strength and thus device and system reliability. Here, we describe a new test specimen for micro-scale tensile strength measurements that allows for direct assessment of surface effects on strength. Specimens were formed from silicon-on-insulator wafers by deep reactive ion etching and tested with instrumented indentation. The experimental results were interpreted using finite element analyses to extract fracture strength. Fracture strengths as great as 3 GPa were observed, with fracture initiating at processing-induced flaws and propagating along {111} and {110} planes.

INTRODUCTION

Microelectromechanical systems (MEMS) have many potential applications, from non-contacting sensors such as accelerometers, gyroscopes, and pressure gauges, to more complicated devices including contacting and rubbing components—one of the few such devices to be commercially viable to date is the digital mirror array used in high-brightness displays [1]. The MEMS sensor market had revenues of $1.5 billion in 2005 and is projected to grow to $4.2 billion by 2012 [2]. This forecast includes a large increase as MEMS sensors are incorporated into cell phones and laptop computers. However, the potential for various contacting and rubbing MEMS devices cannot yet be realized due to a lack of device mechanical reliability. For example, although the strength of single-crystal silicon structures and devices has been demonstrated to reach values as great as 18 GPa [3], the distribution of strength values over test sample populations is usually extremely broad [4], and the stress ranges experienced in MEMS devices in use are likely to vary greatly. As a result, it is helpful to have a form of proof testing to assess, predict, and optimize device reliability [5].

A number of test structures have been developed to measure the strength of MEMS materials that could be used in such proof testing. Traditional tensile tests are a useful configuration due to the uniform stress state produced across the gage section [6, 7, 8, 9, 10]. Other strength measurement techniques include fixed-free beams [11, 12], fixed-fixed beams [3], and biaxial flexure tests [13]. However, in many of these techniques, small gripping, mounting, and loading misalignments can lead to significant experimental errors. As an alternative, Quinn *et al.* developed a micromachined "theta-like" test specimen [14, 15], originally invented by Durelli *et al.* as a macro-scale test method [16], to measure strengths at the micro scale. These test specimens, named for their likeness to the Greek letter theta, demonstrated the viability of the theta-specimen technique, but also illustrated a number of problems: mounting the specimens for testing was difficult, non-ideal loading led to undesirable stress concentrations, and collecting the broken parts after testing for fractography was difficult. In this paper, we describe a new arch theta test specimen for micro-scale tensile strength measurements. For the arch theta specimen, the complex inner geometry of Durelli's original theta design, consisting of three straight sections linked by tangential radii, has been replaced with a simple arch. The specimen was designed with a "top hat" to minimize the effects of misalignments and stress concentrations [17], fabricated using silicon-on-insulator (SOI) wafers to provide better control of device thickness and a more robust base for manipulation and mounting, and tested using a break-detection routine on an instrumented indenter to minimize damage to the specimen after failure.

EXPERIMENTAL METHOD

The fabrication sequence for the arch theta test structure is shown in Fig. 1. The process started with a (001) SOI wafer consisting of a Si device layer (25.0 μm ± 0.5 μm thick), SiO_2 isolation layer (2.0 μm ± 0.1 μm thick), and a Si handle wafer (400 μm ± 10 μm thick). The Si device layer and Si handle wafer were patterned by photolithographic masks and etched using deep reactive ion etching (DRIE) to define the device features. The SOI wafer was oriented such that the web region of the 250 μm diameter test specimen was oriented along the <110> direction. After patterning, the SiO_2 layer was removed locally with a buffered-oxide etching solution to create the freestanding specimens. Finally, each specimen strip, consisting of 10 test specimens, was removed from the wafer using a diamond scribe. The strips were mounted into an aluminum puck using a clamping configuration that allowed the specimens to stand upright and remain isolated from surrounding material. Each test

U.S. Government work not protected by U.S. copyright

specimen was then diametrally compressed via instrumented indentation, which placed the central web section in uniform tension, using a spherical sapphire indenter (radius R = 250 μm) and a break-detection routine that withdrew the indenter on detection of specimen failure to minimize subsequent damage to the specimen. In the routine, the target test displacement rate and break detection trigger displacement rate were 20 nm s^{-1} and 5000 nm s^{-1}, respectively. (It was necessary to set the break detection trigger rate to be rather large to avoid invalid detection from the indenter-to-sample seating jumps that sometimes occurred at the beginning of tests.) Fractography of the broken test specimens was conducted using a field-emission scanning electron microscope (FESEM).

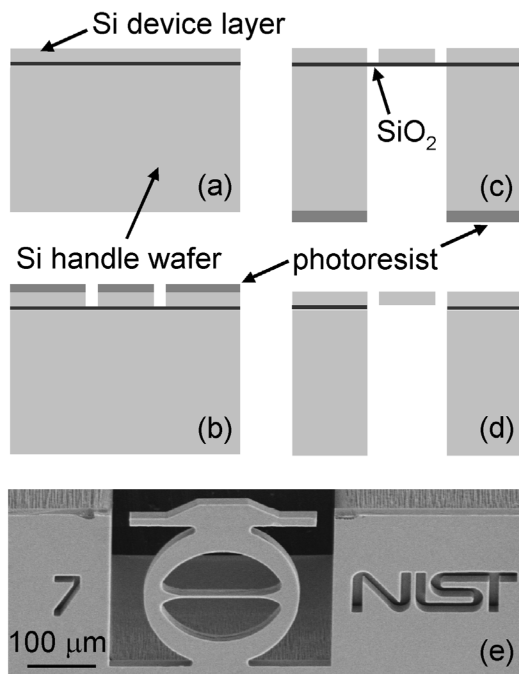

Figure 1. (a)-(d) Schematic diagrams of the fabrication sequence for the arch theta test specimen. (e) Scanning electron micrograph of a completed device.

FINITE ELEMENT ANALYSIS

Finite element analysis (FEA) was used to convert the load P and displacement h at the indenter-to-sample interface to the stress σ and strain ε in the central web section. The elastic properties of silicon were modeled as anisotropic with three independent stiffness components c_{11} = 165.7 GPa, c_{12} = 63.9 GPa, and c_{44} = 79.6 GPa [18], and the sapphire indenter was modeled as an isotropic material with Young's modulus E_{tip} = 400 GPa and Poisson's ratio ν_{tip} = 0.24 [19]. Figure 2 shows the maximum principal stress distribution for an arch theta test specimen subjected to loading with the sapphire indenter. The largest maximum principal stress σ occurs in the web region, and the largest secondary stress σ' is located at the top and bottom of the inner theta region. For this particular geometry, the stress ratio σ'/σ = 0.62 indicates that initial fracture is more likely to occur in the web region. In addition, it is important to note that the inner surface area of the secondary stress region is smaller for the arch theta than for the Durelli theta specimen [17], which further decreases the probability of an unwanted failure outside of the web region. From the FEA simulations, σ [GPa] and ε are found to be related to P [mN] and h [μm] by

$$\sigma = -14.38 \frac{P}{Dt} \tag{1}$$

$$\varepsilon = -0.65 \frac{h}{D}, \tag{2}$$

where D is the arch theta diameter [μm] and t is the device layer thickness [μm]. Equations (1) and (2) are consistent with the idea that as the outer ring is diametrally compressed (negative P and h), the central web section in placed in uniform tension (positive σ and ε). The constants in each equation are different from those describing the original Durelli theta test specimen [16] due to variations in the design (*e.g.*, arch shape for the top and bottom of the inner theta region, addition of the top hat) and material properties (*e.g.*, anisotropic properties for silicon).

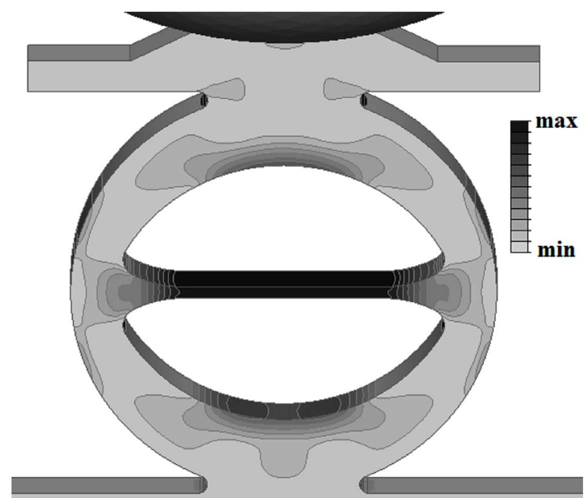

Figure 2. Maximum principal stress distribution for an arch theta test specimen subjected to loading with a sapphire sphere.

RESULTS

Figure 3(a) illustrates a typical P-h curve for an arch theta test specimen loaded to failure. The non-linear region at small P is most likely due to the contacting and seating of the sapphire indenter sphere on the etched surface of the specimen. After the initial seating process, the P-h traces were linear with no discernable hysteresis during five unload-load cycles, which suggests that the mounting and clamping configuration provides a secure and stable test platform. Potential loading misalignment is estimated

to be within 2 μm of the ideal load-point at the center of the 25 μm by 80 μm specimen loading surface. Young's modulus E was determined as the slope of the linear portion of the σ-ε curve; for this particular specimen, E = 176 GPa, which is in good agreement with reported values for silicon in the <110> direction, E = 169 GPa [20]. The fracture strength, the stress at which fracture occurred, was σ_f = 2.2 GPa. As fracture strength is limited by flaw size, a distribution of flaws from the fabrication sequence will result in a strength distribution, and as a result, it is necessary to test a number of samples to quantitatively assess the variability. As shown in Fig. 3(b), the fracture strengths for 24 arch theta test specimens ranged from 2.0 GPa to 3.0 GPa. In brittle materials, such variability is often described by the two-parameter Weibull distribution function,

$$P_f = 1 - \exp\left[-\left(\frac{\sigma_f}{\sigma_\theta}\right)^m\right], \quad (3)$$

in which the characteristic strength σ_θ is the strength that corresponds to a probability of fracture P_f = 63.2% and the Weibull modulus m is a measure of the width of the strength distribution, with large m corresponding to narrow distributions. To fit the data to Eq. (3), the strength values were ranked in ascending order from i = 1 to N, and a P_f was assigned to each value according to $P_f = (i - 0.5)/N$, where N is the number of measurements. The Weibull fit parameters m and σ_θ were then obtained via maximum likelihood estimation. In doing so, m and σ_θ were found to be 18.8 and 2.4 GPa, respectively. These results are consistent with those reported for micromachined single-crystal silicon: σ_f, m, and σ_θ range from 0.5 GPa to 17.5 GPa, 2.7 to 62, and 0.5 GPa to 17.6 GPa [4], respectively.

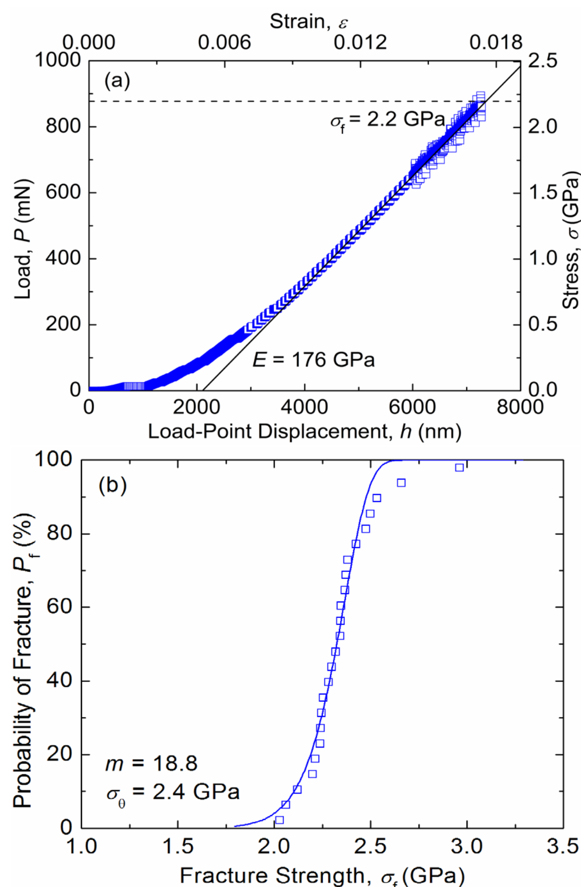

Figure 3. (a) Typical P-h data for an arch theta test specimen loaded to failure. (b) Weibull failure probability plot for the arch theta test specimen.

Fractographic analyses indicated that fracture occurred on the expected silicon cleavage planes. FESEM images of broken web regions, such as the example in Fig. 4, showed fractures originating on either {111} or {110} planes. Single crystal silicon loaded in the <110> direction would likely fracture along the {111} and {110} versus {100} cleavage planes [21]. A close-up of the fracture plane reveals cleavage step hackle, common in single crystal fracture, propagating from the surface-flaw origin, and which chipped out during the fracture process. The critical flaw size a_o can be estimated from

$$a_o = \left(\frac{K_{IC}}{Y\sigma_f}\right)^2, \quad (4)$$

where K_{IC} is the mode I plane strain fracture toughness and Y is a shape factor. K_{IC} = 0.71 MPa $m^{1/2}$ for silicon in the <110> direction [21] and $Y \approx 1.12\pi^{1/2}$ for an edge crack in a semi-infinite specimen [22]. As established in Fig. 3(b), σ_f varies from 2.0 GPa to 3.0 GPa, which corresponds to a_o values of 30 nm to 10 nm, respectively. This flaw size range is much smaller than the average pitch of the DRIE scallops; for this particular DRIE recipe the scallop pitch was about 400 nm. In a systematic study on the effects of DRIE process parameters on etch performance, surface morphology and mechanical behavior, Chen *et al.* identified the fillet radii at the bottom of the etch trenches and the surface roughness from sputtering and redeposition of the photoresistive layer as high stress regions that may ultimately determine the fracture strength [23]. Depending on

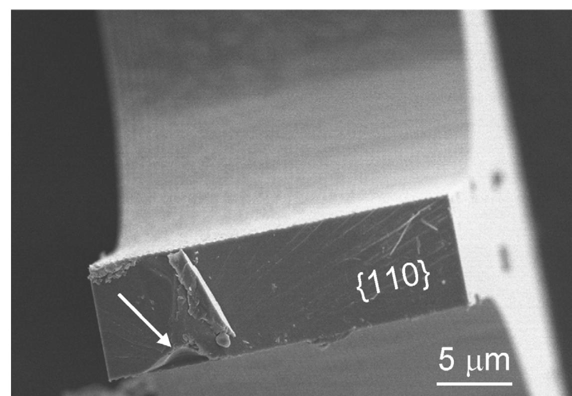

Figure 4. Fracture surface for an arch theta test specimen. Fracture occurred on a {110} plane. The step hackle radiates from the chipped-out region (arrow) where the fracture origin would have been.

the DRIE conditions, the root mean square surface roughness R_{rms} ranged from 5 nm to 50 nm. Since our values for a_o are within these bounds for R_{rms}, it is likely that the processing-induced surface roughness acted as the strength-limiting flaws.

SUMMARY

In summary, we reported on a new arch theta test specimen, which allowed for simple micro-scale strength testing, while removing the difficulties associated with gripping and loading specimens as well as minimizing potential misalignment effects. The fracture strengths for Si specimens ranged from 2.0 GPa to 3.0 GPa and the strength distribution was well-described by a two-parameter Weibull distribution function. The critical flaw sizes were calculated from the observed fracture strengths, and the resulting values suggested that processing-induced surface roughness acted as the strength-limiting flaws. Future work will attempt to identify the strength controlling flaws and their relationship to the processing-induced surface roughness.

ACKNOWLEDGEMENT

The authors thank George D. Quinn of the National Institute of Standards and Technology for his assistance and guidance with regard to fractography and discussions regarding fracture and stress analyses.

REFERENCES

[1] G. T. A. Kovacs, *Micromachined Transducers Sourcebook*. New York: McGraw-Hill, 1998.
[2] "World MEMS sensors markets," *Frost and Sullivan*, Report FA0A-32, 2006.
[3] T. Namazu, Y. Isono, and T. Tanaka, "Evaluation of size effect on mechanical properties of single crystal silicon by nanoscale bending test using AFM," *J. Microelectromech. Syst.,* vol. 9, no. 4, pp. 450-459, 2000.
[4] O. M. Jadaan, N. N. Nemeth, J. Bagdahn, and W. N. Sharpe, Jr., "Probabilistic Weibull behavior and mechanical properties of MEMS brittle materials," *J. Mat. Sci.*, vol. 38, pp. 4087-4113, 2003.
[5] B. L. Boyce, R. Ballarini, and I. Chasiotis, "An argument for proof testing brittle microsystems in high-reliability applications," J. Micromech. Microeng., vol. 18, no. 11, pp. 1-4, 2008.
[6] W. N. Sharpe, B. Yuan, and R. L. Edwards, "A new technique for measuring the mechanical properties of thin films," *J. Microelectromech. Syst.*, vol. 6, no. 3, pp. 193-199, 1997.
[7] W. N. Sharpe, K. T. Turner, and R. L. Edwards, "Tensile testing of polysilicon," *Exp. Mechanics*, vol. 39, no. 3, pp. 162-170, 1999.
[8] W. Suwito, M. L. Dunn, S. J. Cunningham, and D. T. Read, "Elastic moduli, strength, and fracture initiation at sharp notches in etched single crystal silicon microstructures," *J. Appl. Phys.*, vol. 85, no. 7, pp. 3519-3534, 1999.
[9] I. Chasiotis and W. G. Knauss, "A new microtensile tester for the study of MEMS materials with the aid of atomic force microscopy," *Exper. Mech.*, vol. 42, no. 1, pp. 51-57, 2002.
[10] B. L. Boyce, J.M. Grazier, T. E. Buchheit, and M. J. Shaw. "Strength distributions in polycrystalline silicon MEMS," *J. Microelectromech. Syst.*, vol. 16, no. 2, pp. 179-190, 2007.
[11] F. Ericson and J.-A. Schweitz, "Micromechanical fracture strength of silicon," *J. Appl. Phys.*, vol. 68, no. 11, pp. 5840-5844, 1990.
[12] C. J. Wilson and P. A. Beck, "Fracture testing of bulk silicon microcantilever beams subjected to a side load," *J. Microelectromech. Syst.,* vol. 5, no. 3, pp. 142-150, 1996.
[13] K.-S. Chen, A. Ayon, and S. M. Spearing, "Controlling and testing the fracture strength of silicon on the mesoscale," *J. Am. Ceram. Soc.,* vol. 83, no. 6, pp.1476-1484, 2000.
[14] G. D. Quinn, E. Fuller, D. Xiang, A. Jillavenkatesa, L. Ma, D. Smith, and J. Beall, "A novel test method for measuring mechanical properties at the small-scale: the theta specimen," *Cer. Eng. Sci. Proc.,* vol. 26, no. 2, pp. 117-126, 2005.
[15] G. D. Quinn, "Fractographic analysis of miniature theta specimens," *Cer. Eng. Sci. Proc.,* vol. 29, no. 3, pp. 189-199, 2008.
[16] A. J. Durelli, S. Morse, and V. Parks, "The theta specimen for determining tensile strength of brittle materials," *Mat. Res. Standards*, vol. 2, pp. 114-117, 1962.
[17] E. R. Fuller, D. L. Henann, and L. Ma, "Theta-like specimens for measuring mechanical properties at the small-scale: effects of non-ideal loading," *Int. J. Mat. Res.,* vol. 98, no. 8, pp. 729-734, 2007.
[18] W. P. Mason, *Physical Acoustics and the Properties of Solids*. New York: D. Van Nostrand Company, 1958.
[19] B. Holm, R. Ahuja, Y. Yourdshahyan, B. Johansson, and B. I. Lundqvist, "Elastic and optical properties of α- and κ-Al_2O_3," *Phys. Rev. B*, vol. 59, no. 20, pp. 12777-12787, 1999.
[20] W. A. Brantley, "Calculated elastic constants for stress problems associated with semiconductor devices," *J. Appl. Phys.*, vol. 44, no. 1, pp. 534-535, 1973.
[21] R. F. Cook, "Strength and sharp contact fracture of silicon," *J. Mat. Sci.*, vol. 41, pp. 841-872, 2006.
[22] B. Lawn, *Fracture of Brittle Solids*, second ed. Cambridge: Cambridge University Press, 1993.
[23] K.-S. Chen, A. A. Ayon, X. Zhang, and S. M. Spearing, "Effect of process parameters on the surface morphology and mechanical performance of silicon structures after deep reactive ion etching (DRIE)," *J. Microelectromech. Syst.,* vol. 11, no. 3, pp. 264-275, 2002.